An Energy-Conserving Hair Reflectance Model

Article *in* Computer Graphics Forum · June 2011

DOI: 10.1111/j.1467-8659.2011.01976.x · Source: DBLP

5 authors, including:

Eugene d'Eon
NVIDIA
31 PUBLICATIONS **555** CITATIONS
SEE PROFILE

Guillaume François
Weta Digital Ltd.
11 PUBLICATIONS **108** CITATIONS
SEE PROFILE

Jean-Marie Aubry
Weta Digital Ltd.
22 PUBLICATIONS **247** CITATIONS
SEE PROFILE

Eurographics Symposium on Rendering 2011
Ravi Ramamoorthi and Erik Reinhard
(Guest Editors)

Volume 30 (2011), Number 4

An Energy-Conserving Hair Reflectance Model

Eugene d'Eon Guillaume Francois Martin Hill Joe Letteri Jean-Marie Aubry

Weta Digital

Abstract

We present a reflectance model for dielectric cylinders with rough surfaces such as human hair fibers. Our model is energy conserving and can evaluate arbitrarily many orders of internal reflection. Accounting for compression and contraction of specular cones produces a new longitudinal scattering function which is non-Gaussian and includes an off-specular peak. Accounting for roughness in the azimuthal direction leads to an integral across the hair fiber which is efficiently evaluated using a Gaussian quadrature. Solving cubic equations is avoided, caustics are included in the model in a consistent fashion, and more accurate colors are predicted by considering many internal pathways.

Categories and Subject Descriptors (according to ACM CCS): I.3.7 [Computer Graphics]: Three-Dimensional Graphics and Realism—Shading

1. Introduction

Accurately accounting for the reflectance from hair and fur is of considerable importance for the realistic image synthesis of believable characters in film and video games. The first step towards achieving this goal is possessing an accurate model for the reflectance from an individual hair strand. The seminal work on this subject, due to Marschner et al. [MJC*03], presents an analytic factored model based on an internal refracted pathway analysis. This model is widely successful but is based on several simplifying assumptions that limit its accuracy for low-absorbing hair (such as light blond and white hair), for grazing angles of illumination, and for high surface roughness. Nearly a decade ago approximations were chosen to yield the most efficient model possible that was capable of matching measured data. Today, we find it practical to revisit the application of Marschner et al.'s model to rough surfaces, deriving more complex scattering functions that have several desired properties.

2. Related work

In this paper we focus exclusively on physically-based analytic fiber reflectance models. Kajiya and Kay [KK89] presented the first such model. It has been improved upon significantly by Marschner et al. [MJC*03] by considering variation of reflectance in the azimuthal directions and accounting for internal absorption and caustics. The methods of Marschner et al. [MJC*03] have been extended in several papers. Zinke and Weber [ZW07] introduced the formalism of *Bidirectional Curve Scattering Distribution Functions* (BCSDFs) and a near-field model, important for close rendering of hair fibers and global illumination. They also presented a far-field model which is very similar to the azimuthal component of our new model, but with a different treatment of azimuthal roughness.

Zinke et al. [ZRL*09] found that adding a non-physical diffuse term and a parameter to scale the primary reflectance term improved the accuracy of fitting the model of Marschner et al. [MJC*03] to measured data. Sadeghi et al. [SPJT10] presented an artist friendly model which simplifies the use of the Marschner model. These modifications are useful in practice but do not provide a globally energy-conserving model, which is the goal of this paper.

Ogaki et al. [OTS10] present a simulation-driven approach to generating hair reflectance functions based on photon tracing through translucent user-modeled hair-fiber micro-geometry. The resulting reflectance data is stored in tables such as those proposed by Nguyen and Donnelly [ND05] for real-time hair rendering. This method creates energy-conserving models but lacks the control of an analytic parametrized model and requires the user to measure and model the micro-geometry of the desired hair type.

Our model can be efficiently integrated within previous methods for computing multiple scattering within hair volumes [LV00, MM06, ZYWK08, SSD*10]. For an extensive

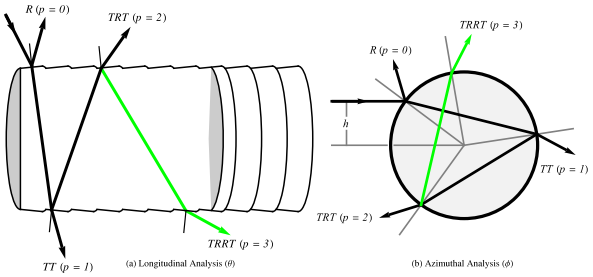

Figure 1: *Refracted pathways through a hair fiber. Single Reflectance (R), double transmittance (TT), and transmission-reflection-transmission (TRT). Our model incorporates a new TRRT term (shown in green).*

review of hair shading, animation and modeling techniques we refer the reader to the survey by Ward et al. [WBK*07].

3. Factored Hair Reflectance Models

A rich set of phenomena is predicted by the analytic model of Marschner et al. [MJC*03] by decomposing the reflectance into separate modes of propagation. They present solutions for the first three modes—the direct reflectance (R), the double transmittance (TT) and the set of pathways with exactly one internal reflection (TRT) (Figure 1). We review the factored pathway analysis of Marschner et al. for smooth hair fibers, which forms the basis of our new model, and subsequently investigate the method of treating surface roughness.

We adopt the notation of Marschner et al. [MJC*03] for parametric hair reflectance models described as a function of *incoming* and *reflected directions*, denoted $\vec{\omega}_i$ and $\vec{\omega}_r$, respectively. The local coordinate system of the hair, $\{\vec{u},\vec{v},\vec{w}\}$, has $\vec{u}$ tangent to the hair in the direction of growth and the plane spanned by $\{\vec{v},\vec{w}\}$ is called the *normal plane*. Symmetry permits a parametrization in terms of *longitudinal* inclinations to the normal plane, θ_i and θ_r, together with the relative *azimuth*, $\phi = \phi_r - \phi_i$. Notation is simplified by referring to the longitudinal *difference angle* $\theta_d = (\theta_r - \theta_i)/2$ and *half angle* $\theta_h = (\theta_r + \theta_i)/2$. The *index of refraction* η of the hair is typically fixed at 1.55. Absorption inside hair is primarily caused by two pigments: eumelanin and pheomelanin with *concentrations* ρ_e and ρ_p respectively. Given the *absorption cross-sections* for eumelanin $\sigma_{a,e}$ and pheomelanin $\sigma_{a,p}$ for each wavelength of light (see Section 6.1), the spectral *absorption coefficient* is $\mu_a = \rho_e\sigma_{a,e} + \rho_p\sigma_{a,p}$.

A *factored reflectance model* $S(\theta_i,\theta_r,\phi)$ exploits the Bravais properties of an idealized smooth circular hair fiber. The total reflectance is decomposed into a sum of contributions indexed by the *number of path segments p* inside the hair before exiting, $p \in \{R=0, TT=1, TRT=2, TRRT=3, \ldots\}$ (see Figure 1). The total reflectance function S is the sum of all such *component scattering functions* S_p

$$S(\theta_i,\theta_r,\phi) = \sum_{p=0}^{\infty} S_p(\theta_i,\theta_r,\phi) \tag{1}$$

each of which is factored into a *longitudinal scattering function* M_p (Figure 1a) and an *azimuthal scattering function* N_p (Figure 1b)

$$S_p(\theta_i,\theta_r,\phi) = M_p(\theta_i,\theta_r)N_p(\theta_i,\theta_r,\phi). \tag{2}$$

For a circular fiber with a smooth surface, the first four scattering functions S_p can be solved for exactly. Effects from elliptical hair fibers, surface roughness, and tilted cuticle scales are introduced approximately by modifying the idealized model in an appropriate fashion.

4. Longitudinal Scattering

In this section we consider the thought experiment of observing a non-absorbing hair fiber in a uniform, white environment. The $1/\eta^2$ solid angle compressions and contractions cancel and all paths lead to white, making the hair indistinguishable from the white background. The analysis of this problem (or, specifically, an equivalent reciprocal problem) is used to show that previous extensions of Marschner et al. [MJC*03] to rough hairs are not energy-conserving for all roughnesses and angles of illumination/viewing. We use the same analysis to demonstrate the energy conservation of our new proposed scattering function.

4.1. The Gaussian M_p Longitudinal Scattering Function

Marschner et al. [MJC*03] propose an efficient method for simulating reflectance from a hair fiber with a rough surface. In the idealized case of a smooth circular hair, light arriving along a single incoming inclination θ_i produces reflected light restricted to the specular cone $\theta_r = -\theta_i$ (Figure 2 left). This yields a longitudinal scattering function $M_p = \delta(\theta_r + \theta_i)$ for all p and is energy conserving. To simulate deviation of reflected directions out of the perfect specular cone due to roughness on the surface of the hair, Marschner et al. [MJC*03] propose using a Gaussian function of the half-angle,

$$M_p = g(\beta_p; \theta_h - \alpha_p), \tag{3}$$

where

$$g(\beta;\theta) = \frac{e^{-\theta^2/(2\beta^2)}}{\sqrt{2\pi}\beta} \tag{4}$$

is a normalized Gaussian of longitudinal inclination θ, β is a roughness term (specifically, the standard deviation of deflection out of the specular cone in the longitudinal direction), and α_p is a simple function of the tilt of the cuticle scales (Figure 1). The angular redistribution of radiance in Equation (3) is non-conservant for several reasons:

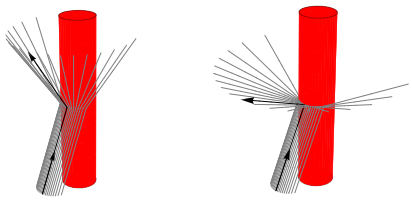

Figure 2: *Rays reflecting off a smooth cylinder are restricted to a single specular cone (left). The longitudinal scattering functions M_p simulate scattering into non-specular cones due to a rough surface. The compression and contraction of these cones involves a net change in radiance. For deflection into angles toward the normal plane (right) the same number of photons enter a wider cone and the radiance decreases.*

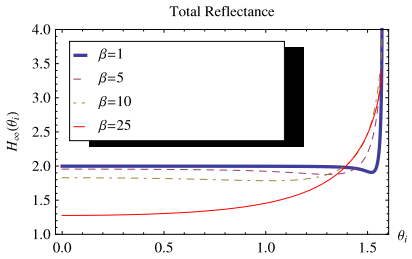

Figure 3: *Total reflectance from cylinders with $\eta = \infty$ and various roughnesses β due to unit incoming radiance at a single angle θ_i. Gaussian longitudinal scattering functions are not energy-conserving. Our new model produces a total reflectance of 1 for all θ_i and β.*

- The Gaussian in Equation (4) is normalized with respect to $\theta \in \{-\infty, \infty\}$ but it is evaluated with $\theta_h \in \{-\pi/2, \pi/2\}$. Also, the use of θ_h instead of θ doubles the reflected energy on average (Figure 3).
- Deflection of light from one specular cone $-\theta_i$ into another θ_r involves a compression or contraction of the cones when $\theta_i \neq -\theta_r$ (see Figure 2). This is only approximately accounted for by a $1/\cos^2\theta_d$ term in Marschner et al. [MJC*03].
- Deflection near grazing illumination angles moves considerable energy into angles outside of the range $\theta \in \{-\pi/2, \pi/2\}$ (angles that will never be received, thereby losing energy).

A characterization of this non-conservant scattering can be seen by considering the total reflectance of an absorption free ($\mu_a = 0$) hair fiber under unit monodirectional illumination. To simplify the analysis, we observe the behaviour of M_R only by having R return all the energy (setting the index of refraction to ∞). The total reflected energy is then

$$H_\infty(\theta_i) = \int_{-\pi}^{\pi} \left[\int_{-\pi/2}^{\pi/2} N_R(\phi) \frac{M_R(\beta_R, \theta_h)}{\cos^2\theta_d} \cos^2\theta_r \, d\theta_r \right] d\phi \tag{5}$$

where

$$N_R(\phi) = (1/4)|\cos(\phi/2)| \tag{6}$$

is the azimuthal scattering function for R and $M_R = g(\beta_R; \theta_h)$ [MJC*03]. Plots of the total refelctance for various levels of surface roughness are shown in Figure 3. The Gaussian M_p function creates extra energy for grazing angles. For small roughnesses, the total energy is near 2 for most values of θ_i (due to using θ_h with a distribution function normalized over θ). This energy doubling was removed by switching to $M_R = g(\beta_R; 2\theta_h)$ [ZW07, ZYWK08]. However, the Gaussian still yields extra energy at grazing angles and energy loss for high roughnesses. The same behaviour arises in other terms, such as TT and TRT. Indeed, Equation (5) is equivalent to considering the total reflectance of an index $\eta = 1.55$ hair, provided $\mu_a = 0$ and α_p and β_p are constant for all p (the longitudinal functions M_p are then all equal and factor out, leaving the unit-integral azimuthal distribution function $\sum_{p=0}^{\infty} N_p(\phi)$ to replace $N_R(\phi)$).

4.2. An Energy-Conserving Longitudinal Scattering Function M_p

We derive a novel longitudinal scattering function that conservatively redistributes reflected radiance amongst directions on the sphere. This is achieved by employing spherical-Gaussian convolution. For use with a factored reflectance model, we derive a purely-longitudinal function by averaging the behaviour in the azimuthal direction. We consider the spherical Gaussian convolution of a Dirac circle on the surface of a sphere. The longitudinal profile of the resulting distribution is our new scattering function. We refer the reader to Appendix A for a complete derivation. The resulting function is

$$M_p(v, \theta_i, \theta_r) = \frac{\operatorname{csch}(1/v)}{2v} e^{\frac{\sin(-\theta_i)\sin\theta_r}{v}} I_0\left[\frac{\cos(-\theta_i)\cos\theta_r}{v}\right] \tag{7}$$

where $v = \beta^2$ is the *roughness variance* and $I_o(x)$ is the modified Bessel function of the first kind. The shape of the new longitudinal scattering function is shown in Figure 4 for various incident angles. It is asymmetric about the specular cone angle, exhibiting an off-specular peak similar to planar BRDFs, and for all roughnesses is energy conserving:

$$H_\infty = \int_{-\pi}^{\pi} \left[\int_{-\pi/2}^{\pi/2} N_R(\phi) M_p(v, \theta_i, \theta_r) \cos\theta_i \, d\theta_i \right] d\phi = 1.$$

Note that all incidence and exitance factors are contained in the one reciprocal function (Equation 7). This is convenient in a rasterization framework, the contribution of a given fiber to a given pixel being proportional to its *coverage* C of the pixel and to the final scattering function S (Equation 1), $CS(\theta_i, \theta_r, \phi)$. The unprojected length of the hair within a pixel, the hair width, the $\cos\theta_i$ and $\frac{1}{\cos^2\theta_d}$ factors required of previous models are absent. The transformation to a BCSDF is straightforward.

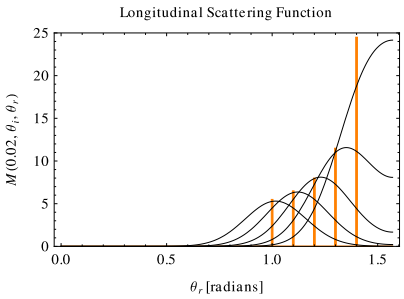

Figure 4: *Shape of our energy-conserving longitudinal scattering function (Equation 7) as a function of exitant direction θ_r for fixed incident directions $\theta_i \in \{-1, -1.1, -1.2, -1.3, -1.4\}$ (radians). The specular cone directions are indicated in orange to illustrate the asymmetry and off-specular peak for large θ. Roughness is fixed at $v = 0.02$ ($\beta = 8.1°$).*

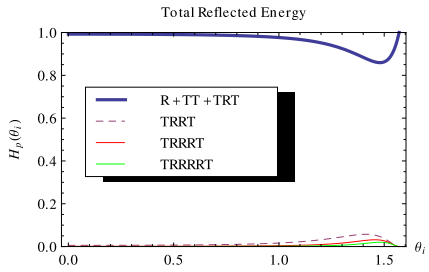

Figure 5: *Total reflectance from a white hair fiber as a function of incoming direction θ_i. Previous models only compute the first three modes of reflectance, R, TT, and TRT, missing almost 15% of the energy at grazing illumination angles. Our new model easily adds additional terms like TRRT.*

5. Azimuthal Scattering

Marschner et al. [MJC*03] analyze the azimuthal scattering behaviour inside a fiber independently from the longitudinal behaviour by exploiting Bravais properties of smooth cylinders. Using a modified index of refraction $\eta' = \frac{\sqrt{\eta^2 - \sin^2\theta_d}}{\cos\theta_d}$, the general analysis can be restricted to an equivalent analysis in the normal plane only. The net change in azimuthal direction Φ is related to the offset $h \in \{-1, 1\}$ from the hair fiber (Figure 1b) and p, the mode of reflection being considered, by

$$\Phi(p,h) = 2p\gamma_t - 2\gamma_i + p\pi, \tag{8}$$

where $\gamma_i = \arcsin(h)$ and $\gamma_t = \arcsin(\frac{h}{\eta'})$.

One method of applying this analysis is the method of solving for h. Given Equation (8), Marschner et al. [MJC*03] solve for all values h that result in light exiting the hair towards the camera (finding h such that $\Phi(p,h) = \phi$). Absorption, Fresnel and derivatives of Equation (8) produce the outgoing radiance along this discrete set of paths. For the R reflection mode, the final N function is simply a cosine (Equation 6). The complexity increases rapidly for higher-order terms. For TT, the single exact h solution is

$$h_{\mathrm{TT}} = \frac{\mathrm{sign}(\phi)\cos(\phi/2)}{\sqrt{1 + a^2 - 2a\,\mathrm{sign}(\phi)\sin(\phi/2)}}$$

where $a = 1/\eta'$. For the TRT paths, either one or three values of h exist for a given ϕ, specifically the solutions of

$$\sin(\phi/2) = -h + 2a^2h^3 + 2ah\sqrt{1-h^2}\sqrt{1-a^2h^2} \tag{9}$$

which exist in closed form, but are quite involved and inconvenient to implement. Closed-form solutions exist for TRRT but not for TRRRT. With significant absorption the higher-order terms $p > 2$ are negligible but for hairs with very low absorption (such as white hair) almost 15% of the reflected energy is due to TRRT and higher-order terms when the angle of incidence is high (Figure 5).

Marschner et al. [MJC*03] use a cubic approximation of Equation (8) when solving for h, reducing the complexity of higher-order terms and offering an approximate method of solution for any desired reflection mode p. However, the accuracy of this approximation has not been validated for large p or for low relative indices of refraction (which arises for hair under water).

In addition to the complexity of requiring root solvers, the approach of solving for h is further limited by singularities caused by caustics, requiring *ad-hoc* user-defined parameters to control them. Additionally, the consideration of discrete azimuthal paths independent of roughness cannot account for the spreading of exitant directions and color shifts that occur as roughness increases. We present an alternative azimuthal scattering function that extends easily to higher order scattering terms, includes caustics in a consistent stable fashion, and exhibits roughness-dependent color shifts.

5.1. Roughened Azimuthal Scattering Functions N_p

We simulate the effects of surface roughness by assuming a Gaussian distribution of deflections in the normal-plane. Each offset h on the fiber produces a continuous distribution of exitant azimuths $D_p(\phi - \Phi(p,h))$. These distributions are Gaussian in ϕ and centered about the discrete azimuths $\Phi(p,h)$ predicted by a smooth hair (Figure 7). The total exitance is found by integrating over the entire fiber

$$N_p(\phi) = \frac{1}{2}\int_{-1}^{1} A(p,h) D_p(\phi - \Phi(p,h))\,dh \tag{10}$$

where $A(p,h)$ is the attenuation along each path due to absorption and Fresnel [MJC*03]. We employ a specialized normalized Gaussian function D_p with an equivalence of all multiples of 2π. Detection at all multiples of 2π is important in order to account for all exitant light, which may undergo several complete azimuthal revolutions inside the hair

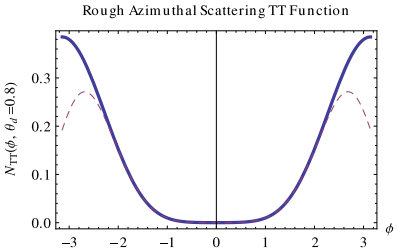

Figure 6: *Rough azimuthal scattering $N_{TT}(\phi)$ with $\theta_d = 0.8$, $\beta_{TT} = 25^\circ$, and $\mu_a = 0$. Previous methods [ZW07] (dashed) transmit approximately half of the expected light in the forward directions $\phi = \pi = -\pi$. This is corrected by using our new Gaussian detector (Equation 11).*

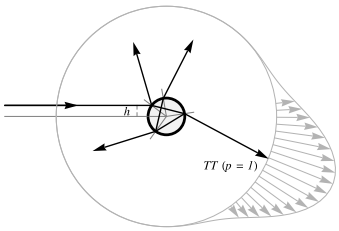

Figure 7: *Rough azimuthal scattering (TT): for each offset h from the hair fiber the exact azimuth $\Phi(p,h)$ predicted by a smooth hair is used to create a Gaussian distribution of exitant azimuths $D_p(\phi - \Phi(p,h))$.*

for $p > 1$. We found that the treatment of Zinke and Weber [ZW07] did not completely resolve this effect (for example, the proximity of the values such as $\pi - \varepsilon$ and $-\pi + \varepsilon$ was not handled, see Figure 6). We call this new distribution function a *Gaussian detector*

$$D_p(\phi) = \sum_{k=-\infty}^{\infty} g(\beta_p; \phi - 2\pi k). \tag{11}$$

The roughness in the normal plane can use the same standard deviations β_p used with the longitudinal functions or use separate parameters for producing anisotropic roughness. As the roughness β approaches 0 the Gaussian detector approaches a Dirac delta function and the scattering functions of Marschner et al. [MJC*03] are recovered starting with Equation (10). In addition to spreading light wider, roughness-dependent color shifts are exhibited when using our new azimuthal scattering function (Figure 8).

6. Final Model and Implementation

For completeness, we provide the remainder of the model (which differs from Marschner et al. [MJC*03] in some respects). The attenuation term for R is a special case

$$A(0,h) = F(\eta, \frac{1}{2}\arccos(\omega_i \cdot \omega_r)). \tag{12}$$

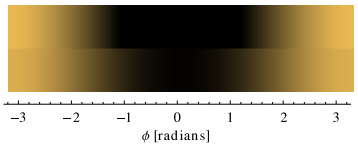

Figure 8: *Azimuthal transmittance color N_{TT} for a smooth hair (top) vs. a rough hair (bottom). Including roughness in the azimuthal direction spreads energy wider. The continuum of absorption lengths contributing to each exitant direction ϕ causes a roughness-dependent color shift.*

where $F(\eta,\theta)$ is Fresnel reflectance and is evaluated using the half-angle for physical consistency. We note that the Bravais Fresnel terms proposed by Marschner et al. [MJC*03] are unnecessary—all other terms can use

$$A(p,h) = (1-f)^2 f^{p-1} T(\mu_a', h)^p \tag{13}$$

which share a common classical Fresnel evaluation

$$f = F(\eta, \arccos(\cos(\theta_d)\cos(\arcsin(h)))). \tag{14}$$

The absorption term $T(\mu_a, h) = \exp(-2\mu_a(1+\cos(2\gamma_t)))$ uses the reduced absorption coefficient $\mu_a' = \mu_a/\cos(\theta_t)$. Effects of cuticle scale tilting can be added by evaluating the longitudinal scattering functions with $M_p(v_p, \theta_i, \theta_r - \alpha_p)$. Note that this is only approximate—the change in length of successive internal bounces due to tilted scales (shown in Figure 1a) is not accounted for. The Gaussian detector (Equation 11) has a closed form representation in terms of the third Eliptic Theta function. In practice it is easiest to implement it with a finite range of k, since higher order terms are negligible for reasonable roughness levels ($\beta < 80^\circ$). We use the following series expansion to evaluate I_0

$$I_0(x) \approx \sum_{i=0}^{10} \frac{x^{2i}}{4^i (i!)^2}. \tag{15}$$

We evaluate Equation (10) using a Gaussian quadrature. We found a quadrature of order 35 is sufficient for all but very smooth hairs ($\beta < 2^\circ$). The N_p functions can be precomputed in 2D tables for each desired combination of μ_a and β_p [ND05]. Furthermore, symmetry can be used to reduce cost by integrating over $h \in \{0,1\}$ and extending the Gaussian detector to detect at both ϕ and $-\phi$. Non-Gaussian roughness can be simulated by approximating a general deflection distribution function as a Gaussian sum.

6.1. RGB Melanin Absorption Cross-Sections

Starting with the analytic approximations for melanin absorption cross-sections given by Donner and Jensen [DJ06], we computed absorption colors using 40 spectral bands, mapping to sRGB based on a D65 illuminant. We found that RGB cross-sections could closely, but not perfectly, match the colors predicted by the spectral model. The values we found are $\sigma_{a,e} = \{0.419, 0.697, 1.37\}$ and $\sigma_{a,p} =$

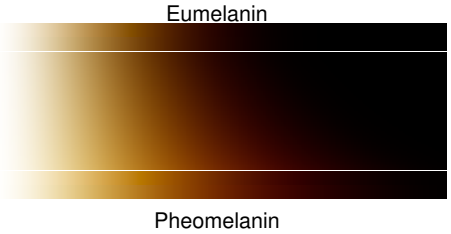

Figure 9: *Transmitted color through eumelanin and pheomelanin mixtures as a function of thickness (increasing to the right). Strips at the top and bottom show pure eumelanin and pheomelanin, respectively, with the top half of each strip showing the spectral reference, and the bottom half showing the RGB approximations.*

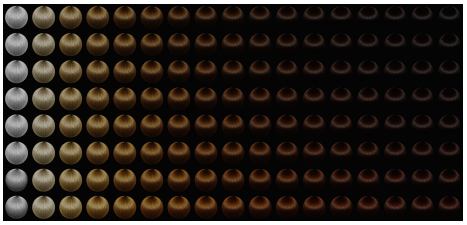

Figure 10: *A range of results using our model with varying mixtures of eumelanin and pheomelanin. The top row shows pure eumelanin, the bottom row shows pure pheomelanin, and total concentration of both increases to the right.*

$\{0.187, 0.4, 1.05\}$ (with units proportional to R^2 such that concentrations near $1/R^3$ give black hair; R being the radius of the hair). The resulting colors are shown in Figure 9. The horizontal bars at the top and bottom of the figure compare spectral absorption calculations to the approximate RGB equivalents. The match is quite close, making the horizontal edge between the two difficult to notice.

7. Results

In this section we present images obtained using a Pixar Photorealistic Renderman implementation of our model. We compute multiple scattering using the Dual Scattering method [ZYWK08] into which our model integrates seamlessly. Figure 11 compares a Dual Scattering simulation of light hair using both Gaussian longitudinal functions ($M_R = g(\beta_R; 2\theta_h)$ to avoid energy doubling) and our spherical Gaussian convolution longitudinal function. Light spreads farther into darker regions with our new scattering function because Dual Scattering approximates multiple-scattering events as a single computation with a large effective roughness. Such high roughnesses are where the Gaussian longitudinal function loses signifant energy (for most angles, as seen in Figure 3).

We demonstrate a full range of hair colors derived from spectrally-matched melanin concentrations, shown in Figure 10. Figure 12 shows a further example of natural, physically-based color, also demonstrating energy-conservant glints that do not require any smoothing controls. Glints can easily be adjusted by modifying the physical properties of the hair fibers, such as rotation and eccentricty similar to Marschner [MJC*03].

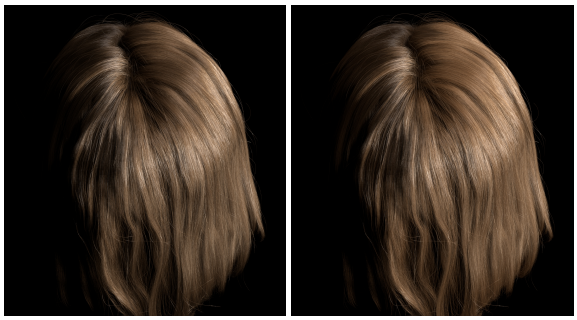

Figure 11: *Light hair rendered using (left) Gaussian longitudinal scattering and (right) our method.*

8. Conclusions and Future Work

We have presented a new factored reflectance model for human hair fibers. Our parametric model is energy-conserving for all roughness and absorption levels and for all angles of illumination. The implementation of our model is straightforward and extends easily to all orders of internal reflection without the requirement for root solvers. We have demonstrated realistic results with our model and implemented it in both real-time and production pipelines. An area for future work is phenomenological comparisons with this new model and its easy extension to non-uniform chromophore distributions, such as including a non-absorbing medulla. Preliminary experiments with this idea led to subtle shifts in color, requiring measurements to validate its practicality. The energy analysis of TRRT and higher order terms suggests that these are not the cause for diffusive colored reflectance observed in hair, as previously suggested. We believe this phenomena must arise due to inner-core scattering, which also desaturates the primary terms. A possible extension to feathers seems promising (Figure 13).

9. Acknowledgments

The authors are indebted to Geoffrey Irving for the trig expansion yielding Equation (9) and for useful discussions related to Section 5. We would also like to thank Jedrzej Wojtowicz, Paolo Selva, Paul Roberts, Michael Nielsen, Luca Fascione, Sebastian Sylwan and the anonymous reviewers.

Figure 12: *Various natural hair colors using our new reflectance model with Dual Scattering. Glints are exhibited in an energy-conserving fashion with no extra control parameters.*

Figure 13: *Future work will consider applying our findings to the rendering of realistic feathers.*

References

[DJ06] DONNER C., JENSEN H. W.: A spectral BSSRDF for shading human skin. In *Rendering Techniques* (2006), pp. 409–417.

[KK89] KAJIYA J., KAY T.: Rendering fur with three dimensional textures. In *Computer Graphics (Proceedings of SIGGRAPH 89)* (1989), vol. 23, ACM, pp. 271–280.

[LV00] LOKOVIC T., VEACH E.: Deep shadow maps. In *Proceedings of SIGGRAPH 2000* (2000), ACM Press/ACM SIGGRAPH, pp. 385–392.

[MJC*03] MARSCHNER S. R., JENSEN H. W., CAMMARANO M., WORLEY S., HANRAHAN P.: Light scattering from human hair fibers. *ACM Trans. Graph. 22* (July 2003), 780–791.

[MM06] MOON J. T., MARSCHNER S. R.: Simulating multiple scattering in hair using a photon mapping approach. *ACM Trans. Graph. 25* (July 2006), 1067–1074.

[ND05] NGUYEN H., DONNELLY W.: Hair animation and rendering in the Nalu demo. In *GPU Gems 2* (2005), Addison-Wesley, pp. 361–380.

[OTS10] OGAKI S., TOKUYOSHI Y., SCHOELLHAMMER S.: An empirical fur shader. In *ACM SIGGRAPH ASIA 2010 Sketches* (2010), ACM, p. 16.

[SPJT10] SADEGHI I., PRITCHETT H., JENSEN H. W., TAMSTORF R.: An artist friendly hair shading system. *ACM Trans. Graph. 29* (July 2010), 56:1–56:10.

[SSD*10] SHINYA M., SHIRAISHI M., DOBASHI Y., IWASAKI K., NISHITA T.: A simplified plane-parallel scattering model and its application to hair rendering. In *2010 18th Pacific Conference on Computer Graphics and Applications* (2010), IEEE, pp. 85–92.

[WBK*07] WARD K., BERTAILS F., KIM T., MARSCHNER S., CANI M., LIN M.: A survey on hair modeling: Styling, simulation, and rendering. *IEEE Transactions on Visualization and Computer Graphics* (2007), 213–234.

[ZRL*09] ZINKE A., RUMP M., LAY T., WEBER A., ANDRIYENKO A., KLEIN R.: A practical approach for photometric acquisition of hair color. *ACM Trans. Graph. 28* (December 2009), 165:1–165:9.

[ZW07] ZINKE A., WEBER A.: Light scattering from filaments. *IEEE Transactions on Visualization and Computer Graphics* (2007), 342–356.

[ZYWK08] ZINKE A., YUKSEL C., WEBER A., KEYSER J.: Dual scattering approximation for fast multiple scattering in hair. *ACM Trans. Graph. 27* (August 2008), 32:1–32:10.

Appendix A: Derivation of the M_p function

The normalized spherical Gaussian of variance v centered in $P \in S^2$ is the function: $x \mapsto g(x,P) = \frac{\operatorname{csch}(1/v)}{2v} e^{\frac{P\cdot x}{v}}$. Averaging along the circle at latitude $\theta_r \in (-\frac{\pi}{2}, \frac{\pi}{2})$ yields

$$G(x) := \frac{1}{2\pi}\int_0^{2\pi} g(x,P)\,d\phi_r.$$

where $P = P(\theta_r, \phi_r)$ in spherical coordinates. If $x = x(\theta_i, \phi_i)$

$$x \cdot P = \cos(\theta_i)\cos(\theta_r)\cos(\phi_i - \phi_r) + \sin(\theta_i)\sin(\theta_r)$$

hence

$$\begin{aligned} G(v) &= \frac{\operatorname{csch}(1/v)}{2v}\frac{e^{\frac{\sin(\theta_i)\sin(\theta_r)}{v}}}{2\pi}\int_0^{2\pi} e^{\frac{\cos(\theta_i)\cos(\theta_r)\cos(\phi_r-\phi_i)}{v}}\,d\phi_r \\ &= \frac{\operatorname{csch}(1/v)}{2v}\frac{e^{\frac{\sin(\theta_i)\sin(\theta_r)}{v}}}{2\pi}\int_0^{2\pi} e^{\frac{\cos(\theta_i)\cos(\theta_r)\cos(\phi_r)}{v}}\,d\phi_r \\ &= \frac{\operatorname{csch}(1/v)}{2v} e^{\frac{\sin(\theta_i)\sin(\theta_r)}{v}} I_0\left[\frac{\cos(\theta_i)\cos(\theta_r)}{v}\right] \end{aligned}$$

Incidence at angle θ_i creates a specular cone at $-\theta_i$ (thus, the negations in Equation 7).